

# Human Gaussian Splatting: Real-time Rendering of Animatable Avatars

Arthur Moreau\*

Jifei Song\*

Helisa Dhano

Richard Shaw

Yiren Zhou

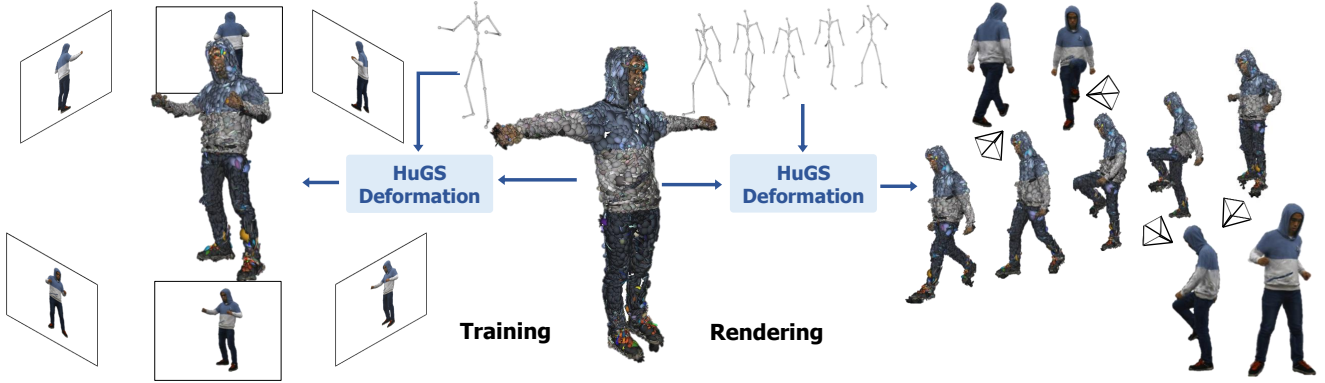
Eduardo Pérez-Pellitero  
Huawei Noah's Ark Lab

Figure 1. **Overview of HuGS.** Using multi-view video frames of a dynamic human, HuGS learns a photorealistic 3D human avatar represented by a 3D Gaussian Splatting model. Given an arbitrary human body pose, our model deforms the canonical 3D representation to the observation space, from which novel views can be rendered in real-time from any camera viewpoint.

## Abstract

This work addresses the problem of real-time rendering of photorealistic human body avatars learned from multi-view videos. While the classical approaches to model and render virtual humans generally use a textured mesh, recent research has developed neural body representations that achieve impressive visual quality. However, these models are difficult to render in real-time and their quality degrades when the character is animated with body poses different than the training observations. We propose the first animatable human model based on 3D Gaussian Splatting, that has recently emerged as a very efficient alternative to neural radiance fields. Our body is represented by a set of gaussian primitives in a canonical space which are deformed in a coarse to fine approach that combines forward skinning and local non-rigid refinement. We describe how to learn our Human Gaussian Splatting (HuGS) model in an end-to-end fashion from multi-view observations, and evaluate it against the state-of-the-art approaches for novel pose synthesis of clothed body. Our method presents a PSNR 1.5dbB better than the state-of-the-art on THuman4 dataset while being able to render at 20fps or more.

\* Authors contributed equally to this work.

## 1. Introduction

Virtual human avatars are essential in virtual reality and video games for applications such as content creation and immersive interaction between users and virtual worlds. The common procedure to create a highly realistic virtual avatar of a person involves expensive sensors and tedious manual work. However, recent progress in 3D modeling and neural rendering enabled to develop machine learning models that learn human avatars from RGB images only.

Recent research in this area focuses on neural representations based on Neural Radiance Fields (NeRF) [21] or Signed Distance Fields (SDF) [24]. Thanks to their continuous design, they can represent highly detailed shape and textures of a clothed human body and thus exhibit better quality than the commonly used textured meshes. However, their deployment in real world applications is difficult, firstly because they present long training and rendering times, but also because animating the character in a controllable way is challenging. As a result, these neural avatars shine on novel view synthesis of body poses observed during training, but struggle to generalize to novel body poses with similar quality.

While animating explicit meshes is a well understood

problem that has been around for decades, *e.g.* using direct skinning algorithms [6, 9, 20], transferring these ideas for implicit neural representations is challenging. Some efforts have been made to learn skinning weights fields, but they define backward skinning methods [27], or need to establish correspondences between observation and canonical space [10, 38], which are pose-dependent problems where solutions are slow and/or do not generalize to unseen body poses, .

In this work, we represent the human body with 3D Gaussian Splatting (3D-GS) [7]. This novel paradigm for view synthesis uses an explicit set of primitives shaped as 3D Gaussians to represent the radiance field of a scene. This enables fast tile-based rasterization, which is orders of magnitudes faster than the rendering speed of implicit methods based on ray marching. Leveraging its explicit and discrete nature, we explore its capability to be deformed with direct forward skinning, similar to a mesh. We observed that using Linear Blend Skinning (LBS) with skinning weights learned for each Gaussian provides an efficient and effective method that generalizes well to new body poses, but is not expressive enough to capture the local garment deformations of loosely clothed avatars. We propose to refine the deformation of Gaussians with a shallow neural network that captures the local and non linear movements of the human body.

The proposed algorithm, named **Human Gaussian Splatting (HuGS)**, is, to the best of our knowledge, the first animatable human body model based on Gaussian Splatting. Our contributions can be summarized as follows:

1. We propose the first algorithm for novel pose synthesis of the human body based on 3D Gaussian Splatting.
2. We define a coarse-to-fine approach to animate the set of Gaussian primitives, based on forward skinning for skeleton-based movements and a pose-dependent MLP for local garments deformations.
3. We compare HuGS to neural-based human representations on two public benchmarks and exhibit results on-par or better than state-of-the-art methods, while rendering one order of magnitude faster, which is crucial for real-world deployment.

## 2. Related work

Due to the nature of our work, in this section we review prior work both on differentiable rendering as well as domain-specific methods that relate to animatable human models.

**Radiance Fields** Learning 3D scene representations for novel view synthesis from 2D images has been very active in the last few years [5, 22, 41] since the seminal work of Mildenhall *et al.* [21]. NeRFs rely on differentiable volu-

metric rendering to jointly learn the color emitted from any point as well as the underlying geometry of the scene. This, in turn, enables to render images from an arbitrary camera viewpoint. NeRF is an implicit representation, *i.e.* a scene-specialized neural network, which has the advantage to be continuous and compact, but also computationally intensive and slow. This aspect can be mitigated by storing information in an explicit way, using voxels grids [33, 36], point clouds [12, 42], tetrahedra [8] or hash tables [1, 23]. While these methods usually assume that the scene is static, it can be adapted to model dynamic content by incorporating the time dimension in the scene representation [11, 25, 30]. These dynamic radiance fields enable to train volumetric representation of humans in movement [4, 29] and to replay an existing video from a new camera viewpoint. All these volumetric approaches rely on ray marching and volumetric rendering [37], requiring to evaluate a neural network on many points along each camera ray and thus present a slow rendering time.

Instead, 3D Gaussian Splatting [7] models the radiance field with an explicit scene representation and a splatting approach. The geometry of the observable scene is approximated by a large number of primitives shaped as 3D gaussians, which are defined by their position, covariance matrix, view-dependent color represented with spherical harmonics, and opacity. All these parameters are optimized through gradient descent to reconstruct the observed images with high fidelity. The main advantage comes from the efficient rendering step that avoids ray marching by sorting and splatting primitives w.r.t. the camera position. Concurrent to our work, there have been several methods dealing with dynamic scenes using gaussian splats. Dynamic 3D Gaussians [18] trains one model per timestep while tracking gaussians positions over time. Deformable 3D Gaussians [43] uses a time-based MLP to deform primitives. 4D Gaussian Splatting [40] combines a MLP with time-dependent voxel features. Finally, Yang *et al* [44] defines 4D primitives that incorporate time in the learnable parametrization. However, deforming 3D gaussians depending on human body pose instead of time has not been explored yet to the best of our knowledge.

**Animatable Human Models** Statistical mesh templates [17, 26] pioneered human body modelling. Fitted to 3D scans of a large set of *unclothed* people, they provide a parametric representation of the human body shape. By using well-known graphic deformation tools, *e.g.* LBS, they can be animated easily, and thus are often used as a building block of more advanced methods. Avatars can be learned from different data modalities, for example using 3D scans [3, 32, 35], monocular videos [39, 45] or a single image [2, 14]. Here, we review methods that use multiview RGB video capture.

Recently, the focus has been to use neural representations to model the human body, either based on NeRF [10, 15, 27, 28, 46] or SDF [13, 38, 47]. Neural Body [28] anchors latent codes to SMPL vertices which are then moved with the template. Neural Actor [15] and Animatable NeRF [27] define a canonical NeRF and learn correspondences from observation to canonical space, either with a deformation field or a blend-weights field. ARAH [38] solves this correspondence problem with a joint root-finding approach and uses a canonical SDF. TAVA [10] combines this root-finding technique with the learning of an implicit forward skinning weights field. In addition with the canonical NeRF, the model also learn pose-depnt ambient occlusion to take into account the color variations caused by garment wrinkles. DVA [31] uses an encoder-decoder architecture that attaches volumetric primitives [16] to the SMPL mesh, enabling real-time rendering. Structured Local Radiance Fields (SLRF) [46] proposes to use local NeRFs defined on SMPL vertices, and moved by LBS. The pose-dependent dynamic deformations are modeled by a conditional VAE [34] that disentangles different garment movements observed from a similar body pose. AvatarRex [47] builds on SLRF body representation and combines it with face and hands models to build an animatable avatar rendered in real-time. Finally, PoseVocab [13] addresses body pose encoding by defining per-joints interpolated features that provides more high-frequency information than global pose vectors. In contrast with these methods, we model our avatar with 3D gaussians. It enables to bypass the observation to canonical correspondence problem and provides efficient rendering.

### 3. Method

Our goal is to reconstruct human avatars from multi-view videos and render images of the reconstructed virtual character from arbitrary camera view and body poses, *i.e.*, novel pose synthesis. An overview of our method is presented in Figure 2.

We train our model from a collection of multiview videos depicting various body poses, captured by  $N$  calibrated cameras during  $T$  timesteps. We pre-compute or assume access to SMPL [17] or SMPL-X [26] parameters, *i.e.*, body shape  $\beta$  and body poses  $\theta_t = (\theta_1, \theta_j, \dots, \theta_J)$  expressed as the 3D rotation of each body joint  $j$ , at timestep  $t$ . We also use foreground segmentation masks.

#### 3.1. Canonical Representation

We represent the canonical human body as a set of volumetric primitives shaped as 3D Gaussians, *i.e.*,  $\mathcal{H} = \{g_i\}$ . Each Gaussian  $g_i$  is parametrized by a set of learnable parameters. Note we drop the  $i$ -th subindex to declutter notation, but each Gaussian is parametrized by its own set of parameters:

- a 3D canonical position  $\mathbf{p}_c = (p_x, p_y, p_z)$ ,
- a 3D orientation, represented by a quaternion  $\mathbf{q}_c$ ,
- a 3D scale  $\mathbf{s} = (s_x, s_y, s_z)$ ,
- a color  $\mathbf{c} = (c_r, c_g, c_b)$ ,
- an opacity scalar value  $o$ ,
- a skinning weight vector  $\mathbf{w} = (w_1, w_j, \dots, w_J)$  that regulates the influence of each body joint  $j$  on how the gaussian moves,
- a latent code  $\mathbf{l}$  that encodes the non-rigid motion.

This builds up from the original 3D Gaussian splatting formulation [7], with the addition of the last 2 parameters that encode the pose-dependent movement of each primitive. We consider scale and opacity consistent across novel views and novel poses. For a given target body pose, we transform canonical position, orientation, and color to the posed space, as described in sections 3.2 and 3.3.

#### 3.2. Deformation with forward skinning.

We use Linear Blend Skinning (LBS) to deform our model. We consider body joints in the canonical space imported from the SMPL template model. Given a body pose  $\theta_t$ , we can compute the rigid transformations  $\mathbf{M}_j \in \text{SE}(3)$  for the  $j$ -th body joint using the kinematic tree. Then, each gaussian’s skinning transformation  $\mathbf{T}_t$  for pose  $\theta_t$  is defined by weight-averaging joint transformations according to skinning weights  $\mathbf{w}$ :

$$\mathbf{T}_t = \sum_{j=1}^J w_j \mathbf{M}_j. \quad (1)$$

The canonical Gaussian position is then transformed to the posed space using  $\mathbf{T}_t$ . We also rotate the gaussian using the rotation component  $\mathbf{R}_t$  of  $\mathbf{T}_t = [\mathbf{R}_t | \mathbf{t}_t]$ .

$$\mathbf{p}_{lbs} = \mathbf{T}_t \mathbf{p}_c \quad \mathbf{q}_{lbs} = \mathbf{R}_t \circ \mathbf{q}_c \quad (2)$$

We apply directly forward skinning on the canonical primitives, similar to mesh deformation in common pipelines, and learn only the skinning weights attached to each Gaussian. In contrast, previous NeRF and SDF approaches, because they rely on ray marching on the posed space, need either backward skinning formulations [27] which is notoriously more difficult, or to solve a root-finding problem before applying forward skinning [10, 38].

#### 3.3. Local non-rigid refinement.

LBS moves the Gaussians towards new body poses and provides excellent generalization to novel poses, but only encodes the rigid deformations of the body joints. Because we want our method to be able to operate on clothed avatars, we also need to model local non-rigid deformations caused by garments. To this end, we compute per-gaussian residual outputs learned by a pose-dependent MLP that can translate, rotate, and change the lightness of the primitive.

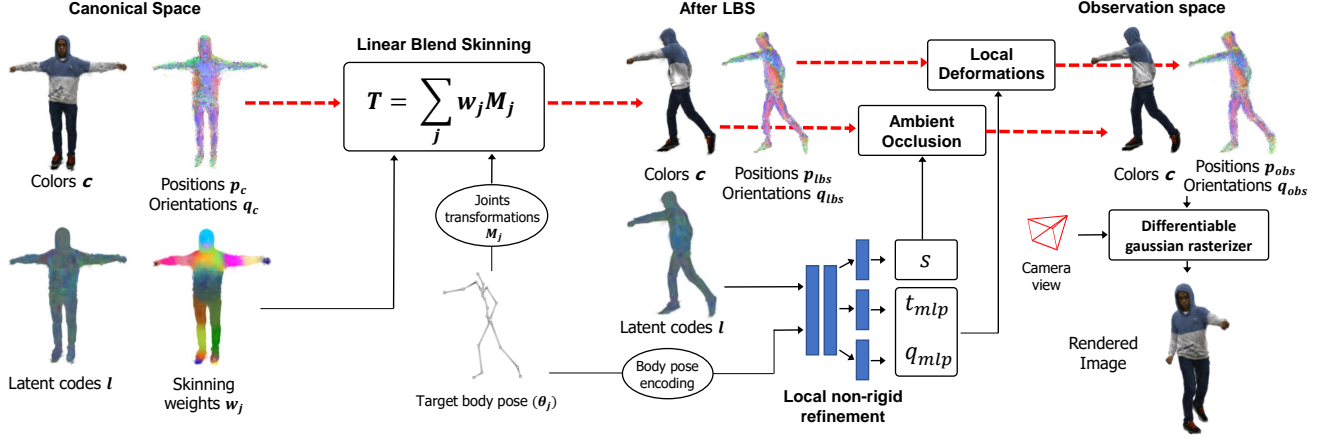


Figure 2. **HuGS method overview.** We represent the different attributes of Gaussians at each step of the deformation pipeline. Canonical positions and orientations are first deformed with LBS using the learned skinning weights. Then positions, orientations, and colors are refined by an MLP using the latent codes. Finally, Gaussians in the observation space are rendered through the target camera view.

**Body pose encoding** We want our model to learn how Gaussians move w.r.t. the body pose instead of time, but we also expect the network to learn *local* deformations. Thus, using the global pose vector  $\theta_t$  as input can represent too many information for local primitives whose position depends on a few joint orientations only. This can ultimately enable the network to learn spurious correlations and overfit [13]. Following SCANimate [32], we use an attention-weighting scheme which uses the skinning weights  $w$  and an explicit attention map  $W$  based on the kinematic tree to define the local pose vector  $\theta_t^l$ :

$$\theta_t^l = (W \cdot w) \odot \theta_t, \quad (3)$$

where  $\theta_t$  is represented as a vector of quaternions and  $\odot$  denotes element-wise multiplication.

**Ambient occlusion** While our approach does not model view-dependent specularities because we consider the human body as Lambertian, we allow the color to change depending on the local body pose. This enables us to take into account self-occlusions and shadows caused by garment wrinkles. This shading effect is referred to as ambient occlusion in graphics pipelines [19]. Formally, the MLP outputs a scaling factor  $s \in [0, 2]$  that multiplies the RGB color of each Gaussian, which is then clipped in  $[0, 1]$ .

**MLP architecture** Our neural network takes as input the local body pose vector  $\theta_t^l$  concatenated with the per-gaussian learnable latent features  $l$ . This latent code identifies each primitive and encodes their local motion depending on the body pose which is then decoded by the MLP. We show in Section 4.4 that using this latent code leads to better performance than using the position. This information is

processed by 2 hidden layers with 64 neurons and ReLU activations and then decoded by 3 separate heads with 2 layers that output respectively a translation vector  $t_{mlp}$ , a quaternion that represents how the Gaussian rotates  $q_{mlp}$  and the ambient occlusion scaling factor  $s$ .

We obtain the final Gaussian position  $p_{obs}$  and orientation  $q_{obs}$  by applying this residual transformation to the LBS output. Importantly, to enable generalization the residual translation vector is defined in the canonical space and thus needs to be rotated with the orientation from LBS.

$$p_{obs} = p_{lbs} + (R_t t_{mlp}) \quad q_{obs} = q_{mlp} \circ q_{lbs} \quad (4)$$

### 3.4. Image rendering.

Once the parameters of Gaussians in the observation space have been computed, we render the image using the fast and differentiable Gaussian rasterizer from 3D-GS [7].

### 3.5. Training procedure.

At each training step, given an image and its corresponding body pose, we transform the canonical Gaussians from the canonical space to the observation space, render the image and finally optimize parameters from the Gaussians and the MLP with gradient descent. We use the SMPL model to initialize the primitives. Gaussian centers are set to the vertices positions, from which we can import the skinning weights from the template. During training, the set of Gaussians is incrementally densified and pruned, following the heuristics proposed by 3D-GS. We describe below the optimization objective of our method, which combines reconstruction and regularization losses. As shown in section 4.4, regularization plays an important role in guiding our over-parametrized model to a solution that generalizes to novel body poses.





Figure 3. **Visualization of MLP outputs.** From left to right: ground-truth image, rendered image, translation output  $t_{\text{mlp}}$  norm (lightest colors indicate largest translation vector) and ambient occlusion factor  $s$  (grey: no color modification, blue: darker colors, red: lighter color). We observe that our MLP learns to operate on the dynamic parts of garments.

**Reconstruction losses** The main training objective of the model is to reconstruct the character in the images. Using the segmentation mask, we set the background pixels from the ground-truth image in black. We use a  $L_1$  loss  $\mathcal{L}_{L_1}$ , a D-SSIM loss  $\mathcal{L}_{\text{ssim}}$  and a perceptual loss  $\mathcal{L}_{\text{lpips}}$  with VGG weights between rendered and groundtruth images.

**Minimize MLP output:** We want our deformations to rely on LBS as much as possible and expect the MLP to learn only local deformations. Thus, we restrict the MLP outputs to be as small as possible. We define one regularization term for each output:  $\mathcal{L}_{\text{trans}}$  controls the norm of the translation residual,  $\mathcal{L}_{\text{rot}}$  pushes the rotation residual close to the identity quaternion  $q_{\text{id}}$ , and  $\mathcal{L}_{\text{amb}}$  guides the ambient occlusion factor to stay close to 1.

$$\mathcal{L}_{\text{trans}} = \|t_{\text{mlp}}\|_2 \quad \mathcal{L}_{\text{rot}} = \|q_{\text{mlp}} - q_{\text{id}}\|_1 \quad \mathcal{L}_s = \|s - 1\|_2 \quad (5)$$

**Regularization of canonical positions:** We encourage Gaussian positions to stay close to the SMPL mesh to avoid floating artifacts. Because our model represents the clothed body, we define a threshold  $\tau_{\text{pos}}$  that represents the maximum distance between the skin and the clothes. We search the nearest vertex  $v_i$  from each Gaussian canonical position  $p_i$  and apply the following loss, that penalizes points that are further than the threshold:

$$\mathcal{L}_{\text{mesh}} = \sum_i \text{ReLU}(\|v_i - p_i\|_2 - \tau_{\text{pos}}) \quad (6)$$

**Skinning weights weak supervision:** Because we train on a limited amount of gestures, the training data can usually be fitted with skinning weights that do not generalize well. Consequently, we softly supervise the skinning weights of our Gaussians with those from SMPL, *i.e.*, the closer a Gaussian is from a vertex, the more similar its skinning weights need to be:

$$\mathcal{L}_{\text{skn}} = \sum_i \text{ReLU}(\|w(g_i) - w(v_i)\|_2 - \tau_{\text{skn}}\|v_i - p_i\|_2) \quad (7)$$

It should be noted that we do not backpropagate the gradient of the distance  $\|v_i - p_i\|_2$  through this loss.

We sum all the reconstruction and regularization terms to obtain the final loss  $\mathcal{L}$ . The weights and hyperparameters used are given in the supplementary materials.

$$\mathcal{L} = \lambda_{L_1}\mathcal{L}_{L_1} + \lambda_{\text{ssim}}\mathcal{L}_{\text{ssim}} + \lambda_{\text{lpips}}\mathcal{L}_{\text{lpips}} + \lambda_{\text{trans}}\mathcal{L}_{\text{trans}} + \lambda_{\text{rot}}\mathcal{L}_{\text{rot}} + \lambda_s\mathcal{L}_s + \lambda_{\text{mesh}}\mathcal{L}_{\text{mesh}} + \lambda_{\text{skn}}\mathcal{L}_{\text{skn}} \quad (8)$$

## 4. Experiments

In section 4.3, we compare Human Gaussian Splatting against state-of-the-art human avatars by reproducing novel pose synthesis experiments from previous work on public datasets. Then, we perform several ablation studies in section 4.4 to show the benefit our design choices. This research has been conducted only with public datasets, which, to the best of our knowledge, have collected human subject data according to regulations. More results are shown in supplementary materials, including videos of novel pose synthesis and a demonstration of real-time rendering.

### 4.1. Implementation Details

Our algorithm is implemented in the PyTorch machine-learning framework. Specifically, the linear blend skinning module is inspired by the SMPL-X repository [26]. For the image rasterization module, we take CUDA kernels from the official 3D-GS [7] implementation for image rendering under a given viewpoint. We optimize the total training objectives using Adam optimizer with hyperparameters  $\beta_1 = 0.9$  and  $\beta_2 = 0.99$ . More implementation details are given in the supplementary materials.

### 4.2. Dataset and Evaluation Metrics

**Dataset** We validate our method on both the THuman4 dataset [46] and the ZJU-Mocap dataset [28]. The THuman4 dataset is captured by 24 well-calibrated RGB cameras covering 3 different subjects. All the multi-view videos are captured at 30 fps, under the image resolution of  $1330 \times 1150$ , ranging from 2500 to 5000 frames. Similarly, ZJU-Mocap dataset is obtained using 23 hardware-synchronized cameras, with  $1024 \times 1024$  resolution. We evaluate novel view and novel pose rendering for reconstructed human avatars on both datasets.

**Evaluation Metrics** Similar to existing dynamic neural human methods, we utilize PSNR, SSIM, and LPIPS to

Table 1. **Quantitative comparison on Thuman4 dataset.** We evaluate the performance on both novel view and novel pose synthesis, and time efficiency. Our method achieves the best performance on all the metrics and supports real-time rendering in the inference stage.

Method	Training poses				Novel poses				Efficiency	
	PSNR	SSIM	LPIPS	FID	PSNR	SSIM	LPIPS	FID	Render (s)	Training (h)
<b>HuGS(Ours)</b>	<b>35.05</b>	<b>0.99</b>	<b>0.020</b>	<b>9.48</b>	<b>32.49</b>	<b>0.984</b>	<b>0.019</b>	<b>11.76</b>	<b>0.05</b>	10
PoseVocab [13]	34.23	0.99	<b>0.014</b>	23.957	30.97	0.977	<b>0.017</b>	37.239	3	48+
SLRF [46]	25.27	0.97	0.024	44.49	26.15	0.969	0.024	110.651	5	25
TAVA [10]	23.93	0.97	0.029	75.46	26.61	0.968	0.032	99.947	-	-
Ani-NeRF [27]	23.19	0.97	0.033	85.45	22.53	0.964	0.034	102.233	1.09	<b>12</b>
ARAH [38]	22.02	0.96	0.033	74.30	21.77	0.958	0.037	77.840	10	36

evaluate both novel view and novel pose synthesis. Moreover, we further include FID metric to measure the realism between the rendering and ground truth photo, following PoseVocab [13].

### 4.3. Comparison with state-of-the-art

**Baselines** We compare our approach with state-of-the-art methods of dynamic human modeling, including 1) PoseVocab [13], which learns joint-structured pose embedding for the human modeling, 2) SLRF [46], uses hundreds of local NeRFs defined on SMPL nodes to preserve the structure information, 3) TAVA [10], a template-free neural actor creation pipeline, 4) Ani-NeRF [27], designing a blend-weight neural field to animate the neural actor and 5) ARAH [38], where articulated SDF is further introduced to help human modeling.

#### 4.3.1 Evaluation on THuman4 dataset

We first report experiment results on “subject00” sequence of the THuman4 dataset [46], where one of the 24 cameras is held out for the evaluation of novel view synthesis. In the novel pose scenario, the method is trained with the first 2000 frames and evaluated on the rest 500 frames. Quantitative results are given in Tab. 1, where the score of other methods is reported from PoseVocab [13] and the efficiency metrics have been collected on each respective paper, except for TAVA that does not report rendering time and indicates training time as a limitation. As we can see from Tab. 1, our method obtains better PSNR, SSIM, and FID scores than all the competitors. In terms of time efficiency, the training time of our method is on par with or better with the baselines, while being the only method to present a real-time rendering in the inference stage. The comparison shows that our method can achieve state-of-the-art performance on both novel view synthesis and novel pose animation while maintaining real-time rendering speed.

We show a qualitative comparison against the best competitor PoseVocab in Figure 5. HuGS and PoseVocab exhibit different strengths and weaknesses. Our method shows more fidelity to the groundtruth image, for example the logo on the hoodie or the head pose which is perfectly aligned.

On the other hand, PoseVocab exhibits a smoother surface thanks to SDF formulation. Another drawback of PoseVocab are artefacts that appears outside of the body topology, due to failure in the inverse skinning process. Because we use forward deformation, such artefacts do not happen with our method.

#### 4.3.2 Evaluation on ZJU-MoCap dataset

We further benchmark our method on ZJU-MoCap dataset [28], where we follow the setting of NeuralBody [28] and report results given by SLRF [46], and use only 4 out of 21 cameras to train the neural human rendering methods, which is a challenging setup for 3D Gaussian splatting approach where dense cameras are required. On this dataset, we train only for 50k iterations because we observe that textures degrade on novel poses with further training, due to the sparse camera setup. Table 2 presents the quantitative comparison between our method and all the baselines. Our method achieves the second-best performance on novel view scenarios and the best performance on novel pose synthesis, where we obtain the highest PSNR and competitive SSIM measures. Moreover, our approach requires the least time consumption and enables real-time rendering compared to all the other baseline methods. The result on the ZJU-MoCap dataset, as well as the qualitative comparison against Neural Body [28] displayed in Figure 4, shows that HuGS can generalize well in novel pose animation tasks.

Table 2. **Quantitative results on ZJU-MoCap dataset.** We present the second-best performance on novel view synthesis while outperforming all the baseline methods on the PSNR metric for novel pose rendering.

Method	Novel Views		Novel Poses	
	PSNR	SSIM	PSNR	SSIM
<b>HuGS(Ours)</b>	26.58	0.934	<b>23.69</b>	0.896
SLRF [46]	<b>28.32</b>	<b>0.953</b>	23.61	<b>0.905</b>
Neural Body [28]	25.79	0.928	21.60	0.870
Ani-NeRF [27]	24.38	0.903	21.29	0.860

#### 4.4. Ablation studies

**Animate with a single transformation** The core of our method consists in combining two transformations: Linear Blend Skinning and a pose-dependent MLP. We study the performance of our method by using either LBS or MLP as the only deformation. Qualitative are shown in Fig. 6. Using only LBS is a strong baseline quantitatively competitive with the state-of-the-art. However, because it only encodes the rigid deformations of body joints, it is not able to model wrinkles on garments and shows a blurrier avatar that lacks details compared to the proposed method. The MLP only version fails to model large deformations such that arms are not represented and thus is not a suitable algorithm for animatable avatars.

**Learning skinning weights** One of the main contributions of our work is to learn per-gaussian skinning weights. We compare this design choice to a simpler baseline: a model where weights are not learned but only copied from the closest SMPL vertex. Because the MLP can potentially correct errors from previous steps, we deactivate it for this experiment and deform gaussians only with LBS. We present the quantitative comparison in Tab. 3, where we can observe that the model with learned skinning weights can bring more than 1dB improvement on PSNR over the ablated version with the SMPL skinning weights. The main reason is that SMPL skinning weights are defined on the naked body while ours can adapt to the particular motion of each primitive belonging to clothes with regard to body joints motion. Template weights could also be inaccurate due to the pose estimation error in the training data, causing misalignment between the body pose and shape and the ground truth image. In comparison, our model with learned skinning weights can overcome this issue by further adapting the learned weights to the input human, thus showing better reconstruction performance.

**Latent code or position** We use a per-gaussian latent code as input of our pose-dependent MLP. It is in contrast

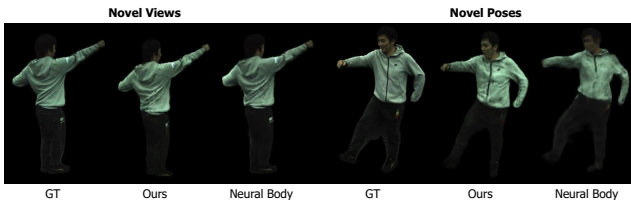


Figure 4. **Comparison with Neural Body on ZJU-MoCap dataset.** While results in novel pose synthesis are comparable for both methods, HuGS generalizes way better to novel poses thanks to its forward deformation formulation.

Table 3. **Ablation study on skinning weights.** We evaluated the ablated model with learned skinning weights and weights from the SMPL template on novel view synthesis.

Method	PSNR	SSIM	LPIPS	FID
Learned	31.99	0.984	0.020	27.15
Template	30.97	0.981	0.022	28.50

with previous work [43] that used the position to identify the primitive and process the deformation. We train a model where we replace the latent code with the position encoding of the canonical position of each Gaussian’s center. As shown in Tab. 4, our model with latent feature embedding can outperform the alternative embedding with position encoding on all the metrics. This is because position encoding on the center of each Gaussian in canonical space could over-constrain the movement as the deformation might not be smoothly correlated to the spatial position, where in contrast, our model with designed latent code can learn the meaningful embedding adaptively to refine each motion.

Table 4. **Ablation study on the design of non-rigid motion refinement.** We compare our model where we input learned latent code to the non-rigid pose refinement module along with the pose embedding, with the alternative method replacing the latent code with the position encoding of the center of 3D Gaussians in canonical space, for novel pose synthesis on THuman4 Dataset.

Method	PSNR	SSIM	LPIPS	FID
Latent code	32.49	0.984	0.019	11.76
Position	32.20	0.985	0.019	17.78

#### 4.5. Efficiency

One of the main advantage of our method against compared methods is its rendering time. Given body joints orientations and camera pose, we render an image of size 512x512 in 50ms or 20fps on a single Tesla V100 GPU. This runtime is an order of magnitude faster than the compared SoTA, as shown in Table 1. Computing transformations from canonical to observation space takes 48ms and gaussians rasterization 2ms.

Moreover, for many applications of animatable avatars, this time can be greatly reduced by pre-computing transformations offline before rendering. This is the case when the avatar only needs to be rendered with a pre-defined set of gestures. In this scenario, each body pose can be stored as a static 3D-GS model and novel views can be rendered in potentially 2ms. Our avatar models contains usually around 40k gaussians, that corresponds to a memory footprint of 2.2MB per frame that need to be cached in memory.

Training the model for our experiments takes from 5 to 20 hours on a Tesla V100, depending on the dataset size. When the number of training frames is small enough, we

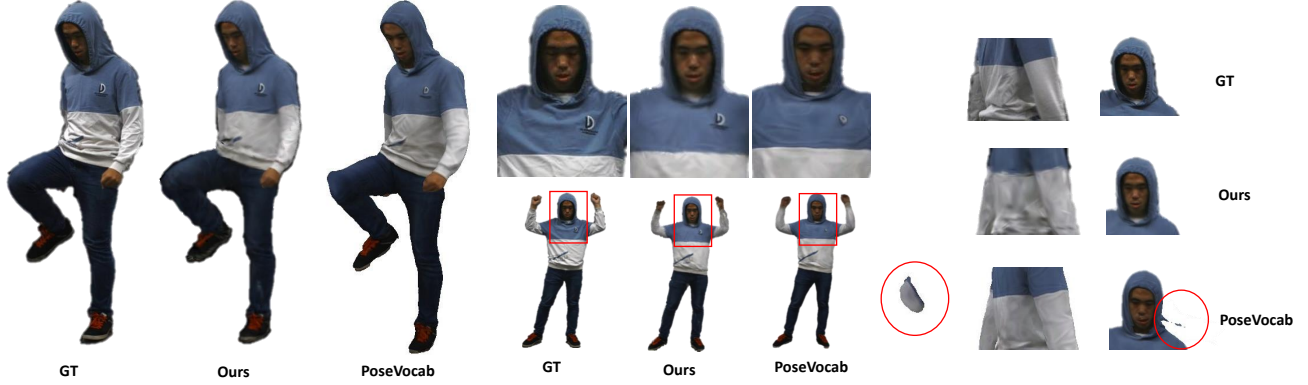


Figure 5. **Qualitative comparison between PoseVocab and HuGS on THuman4 dataset.** On the left, our avatar shows better fidelity w.r.t. the body pose than PoseVocab that fails to deform the hood and the knee at the correct location. In the middle, HuGS presents a more detailed logo and more accurate head pose. On the right, PoseVocab presents artefacts due to failures of the inverse skinning process.

cache the training dataset in memory enabling 4 times faster training iterations than loading images on the fly. It compares equally or favorably to neural rendering competitors. In particular, PoseVocab [13] that presents second higher results on THuman4 requires several days of training.

## 5. Discussion

**Limitations and future work** Our method has shown state-of-the-art performance on novel pose synthesis for dynamic humans with high time efficiency. However, there are still limitations in our algorithm: 1) the 3D reconstruction quality degrades when the camera setup becomes sparse. In this case, the model can overfit to the training observations and fail to render novel poses with high visual quality. 2)

Learning correct garment deformations depending on the body pose is a very challenging problem and solving it with learning-based approaches is difficult. Our deformation module could be further improved by incorporating more physics priors of humans and clothes. 3) Each 3D Gaussian in our human body is optimized and deformed independently, ignoring the intrinsic relation between Gaussians in local neighbourhoods. We think that defining structure and connectivity between primitives could help our model and we leave it as future work.

**Potential societal impacts** The proposed algorithm could be used in Deep Fakes pipelines to synthesize fake videos of people with reenactment for malicious purpose. This aspect needs to be addressed carefully before any deployment.

## 6. Conclusion

In this paper, we have proposed **HuGS**, the first approach for creating and animating virtual human avatars based on Gaussian Splatting. Our approach defines a coarse-to-fine deformation module that combines linear blend skinning with local learning-based refinement. Using Gaussian Splatting for this problem not only help to accelerate rendering, but also enables to bypass difficult inverse skinning approaches required in NeRF-based formulations. As a result, our forward deformation algorithm does not present artefacts caused by failures of inverse approaches and present good generalization properties. Extensive experiment results on dynamic human benchmarks demonstrate that our approach can achieve state-of-the-art human neural rendering performance. Moreover, the proposed algorithm enables real-time rendering, at 20fps if the set of gestures can not be pre-defined and stored, and even more in most applications. These properties should facilitate its deployment for real-world applications.

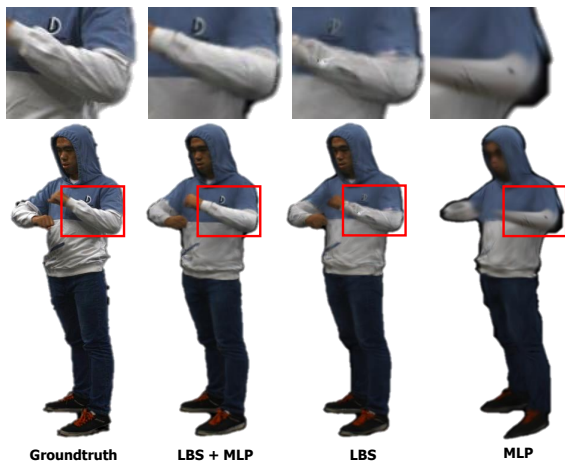


Figure 6. **Ablation study on the importance of combining LBS and MLP.** We show the images in the order of ground truth, qualitative results of our full model with both LBS and posed-based MLP, and the ablated model with LBS only and with MLP only.



## References

- [1] Jonathan T. Barron, Ben Mildenhall, Dor Verbin, Pratul P. Srinivasan, and Peter Hedman. Zip-nerf: Anti-aliased grid-based neural radiance fields. *ICCV*, 2023. 2
- [2] Pol Caselles, Eduard Ramon, Jaime Garcia, Xavier Giro-i Nieto, Francesc Moreno-Noguer, and Gil Triginer. Sira: Re-lightable avatars from a single image. In *Proceedings of the IEEE/CVF Winter Conference on Applications of Computer Vision*, pages 775–784, 2023. 2
- [3] Xu Chen, Yufeng Zheng, Michael J Black, Otmar Hilliges, and Andreas Geiger. Snarf: Differentiable forward skinning for animating non-rigid neural implicit shapes. In *International Conference on Computer Vision (ICCV)*, 2021. 2
- [4] Mustafa Işık, Martin Rünz, Markos Georgopoulos, Taras Khakhulin, Jonathan Starck, Lourdes Agapito, and Matthias Nießner. Humanrf: High-fidelity neural radiance fields for humans in motion. *ACM Transactions on Graphics (TOG)*, 42(4):1–12, 2023. 2
- [5] Youngkyoon Jang, Jiali Zheng, Jifei Song, Helisa Dharmo, Eduardo Pérez-Pellitero, Thomas Tanay, Matteo Maggioni, Richard Shaw, Sibi Catley-Chandar, Yiren Zhou, et al. Vschh 2023: A benchmark for the view synthesis challenge of human heads. In *Proceedings of the IEEE/CVF International Conference on Computer Vision*, pages 1121–1128, 2023. 2
- [6] Ladislav Kavan, Steven Collins, Jiří Žára, and Carol O’Sullivan. Skinning with dual quaternions. In *Proceedings of the 2007 symposium on Interactive 3D graphics and games*, pages 39–46, 2007. 2
- [7] Bernhard Kerbl, Georgios Kopanas, Thomas Leimkühler, and George Drettakis. 3d gaussian splatting for real-time radiance field rendering. *ACM Transactions on Graphics*, 42(4), 2023. 2, 3, 4, 5, 1
- [8] Jonas Kulhanek and Torsten Sattler. Tetra-NeRF: Representing neural radiance fields using tetrahedra. *arXiv preprint arXiv:2304.09987*, 2023. 2
- [9] J. P. Lewis, Matt Corder, and Nickson Fong. Pose space deformation: a unified approach to shape interpolation and skeleton-driven deformation. *Proceedings of the 27th annual conference on Computer graphics and interactive techniques*, 2000. 2
- [10] Ruilong Li, Julian Tanke, Minh Vo, Michael Zollhofer, Jürgen Gall, Angjoo Kanazawa, and Christoph Lassner. Tava: Template-free animatable volumetric actors. 2022. 2, 3, 6
- [11] Zhengqi Li, Simon Niklaus, Noah Snavely, and Oliver Wang. Neural scene flow fields for space-time view synthesis of dynamic scenes. In *Proceedings of the IEEE/CVF Conference on Computer Vision and Pattern Recognition (CVPR)*, 2021. 2
- [12] Zhuopeng Li, Lu Li, and Jianke Zhu. Read: Large-scale neural scene rendering for autonomous driving. In *Proceedings of the AAAI Conference on Artificial Intelligence*, pages 1522–1529, 2023. 2
- [13] Zhe Li, Zerong Zheng, Yuxiao Liu, Boyao Zhou, and Yebin Liu. Posevocab: Learning joint-structured pose embeddings for human avatar modeling. In *ACM SIGGRAPH Conference Proceedings*, 2023. 3, 4, 6, 8
- [14] Tingting Liao, Xiaomei Zhang, Yuliang Xiu, Hongwei Yi, Xudong Liu, Guo-Jun Qi, Yong Zhang, Xuan Wang, Xianguyu Zhu, and Zhen Lei. High-Fidelity Clothed Avatar Reconstruction from a Single Image. In *Proceedings of the IEEE/CVF Conference on Computer Vision and Pattern Recognition (CVPR)*, 2023. 2
- [15] Lingjie Liu, Marc Habermann, Viktor Rudnev, Kripasindhu Sarkar, Jiatao Gu, and Christian Theobalt. Neural actor: Neural free-view synthesis of human actors with pose control. *ACM Trans. Graph.(ACM SIGGRAPH Asia)*, 2021. 3
- [16] Stephen Lombardi, Tomas Simon, Gabriel Schwartz, Michael Zollhofer, Yaser Sheikh, and Jason Saragih. Mixture of volumetric primitives for efficient neural rendering. *ACM Trans. Graph.*, 40(4), 2021. 3
- [17] Matthew Loper, Naureen Mahmood, Javier Romero, Gerard Pons-Moll, and Michael J. Black. SMPL: A skinned multi-person linear model. *ACM Trans. Graphics (Proc. SIGGRAPH Asia)*, 34(6):248:1–248:16, 2015. 2, 3
- [18] Jonathon Luiten, Georgios Kopanas, Bastian Leibe, and Deva Ramanan. Dynamic 3d gaussians: Tracking by persistent dynamic view synthesis. In *3DV*, 2024. 2
- [19] Àlex Méndez-Feliu and Mateu Sbert. From obscurances to ambient occlusion: A survey. *The Visual Computer*, 25:181–196, 2009. 4
- [20] Bruce Merry, Patrick Marais, and James Gain. Animation space: A truly linear framework for character animation. *ACM Transactions on Graphics (TOG)*, 25(4):1400–1423, 2006. 2
- [21] Ben Mildenhall, Pratul P. Srinivasan, Matthew Tancik, Jonathan T. Barron, Ravi Ramamoorthi, and Ren Ng. Nerf: Representing scenes as neural radiance fields for view synthesis. In *ECCV*, 2020. 1, 2
- [22] Ansh Mittal. Neural radiance fields: Past, present, and future. *arXiv preprint arXiv:2304.10050*, 2023. 2
- [23] Thomas Müller, Alex Evans, Christoph Schied, and Alexander Keller. Instant neural graphics primitives with a multiresolution hash encoding. *ACM Trans. Graph.*, 41(4):102:1–102:15, 2022. 2
- [24] Jeong Joon Park, Peter Florence, Julian Straub, Richard Newcombe, and Steven Lovegrove. Deepsdf: Learning continuous signed distance functions for shape representation. In *Proceedings of the IEEE/CVF conference on computer vision and pattern recognition*, pages 165–174, 2019. 1
- [25] Keunhong Park, Utkarsh Sinha, Jonathan T Barron, Sofien Bouaziz, Dan B Goldman, Steven M Seitz, and Ricardo Martin-Brualla. Nerfies: Deformable neural radiance fields. In *Proceedings of the IEEE/CVF International Conference on Computer Vision*, pages 5865–5874, 2021. 2
- [26] Georgios Pavlakos, Vasileios Choutas, Nima Ghorbani, Timo Bolkart, Ahmed A. A. Osman, Dimitrios Tzionas, and Michael J. Black. Expressive body capture: 3D hands, face, and body from a single image. In *Proceedings IEEE Conf. on Computer Vision and Pattern Recognition (CVPR)*, pages 10975–10985, 2019. 2, 3, 5, 1
- [27] Sida Peng, Juntao Dong, Qianqian Wang, Shangzhan Zhang, Qing Shuai, Xiaowei Zhou, and Hujun Bao. Animatable neural radiance fields for modeling dynamic human bodies. In *ICCV*, 2021. 2, 3, 6

- [28] Sida Peng, Yuanqing Zhang, Yinghao Xu, Qianqian Wang, Qing Shuai, Hujun Bao, and Xiaowei Zhou. Neural body: Implicit neural representations with structured latent codes for novel view synthesis of dynamic humans. In *CVPR*, 2021. 3, 5, 6
- [29] Sida Peng, Yunzhi Yan, Qing Shuai, Hujun Bao, and Xiaowei Zhou. Representing volumetric videos as dynamic mlp maps. In *CVPR*, 2023. 2
- [30] Albert Pumarola, Enric Corona, Gerard Pons-Moll, and Francesc Moreno-Noguer. D-NeRF: Neural Radiance Fields for Dynamic Scenes. In *Proceedings of the IEEE/CVF Conference on Computer Vision and Pattern Recognition*, 2020. 2
- [31] Edoardo Remelli, Timur Bagautdinov, Shunsuke Saito, Chenglei Wu, Tomas Simon, Shih-En Wei, Kaiwen Guo, Zhe Cao, Fabian Prada, Jason Saragih, et al. Drivable volumetric avatars using texel-aligned features. In *ACM SIGGRAPH 2022 Conference Proceedings*, pages 1–9, 2022. 3
- [32] Shunsuke Saito, Jinlong Yang, Qianli Ma, and Michael J. Black. SCANimate: Weakly supervised learning of skinned clothed avatar networks. In *Proceedings IEEE/CVF Conf. on Computer Vision and Pattern Recognition (CVPR)*, 2021. 2, 4
- [33] Sara Fridovich-Keil and Alex Yu, Matthew Tancik, Qinlong Chen, Benjamin Recht, and Angjoo Kanazawa. Plenoxels: Radiance fields without neural networks. In *CVPR*, 2022. 2
- [34] Kihyuk Sohn, Honglak Lee, and Xinchun Yan. Learning structured output representation using deep conditional generative models. In *Advances in Neural Information Processing Systems*. Curran Associates, Inc., 2015. 3
- [35] Zhaoqi Su, Liangxiao Hu, Siyou Lin, Hongwen Zhang, Shengping Zhang, Justus Thies, and Yebin Liu. Caphy: Capturing physical properties for animatable human avatars. In *Proceedings of the IEEE/CVF International Conference on Computer Vision*, pages 14150–14160, 2023. 2
- [36] Cheng Sun, Min Sun, and Hwann-Tzong Chen. Direct voxel grid optimization: Super-fast convergence for radiance fields reconstruction. In *CVPR*, 2022. 2
- [37] Andrea Tagliasacchi and Ben Mildenhall. Volume rendering digest (for nerf). *arXiv preprint arXiv:2209.02417*, 2022. 2
- [38] Shaoqi Wang, Katja Schwarz, Andreas Geiger, and Siyu Tang. Arah: Animatable volume rendering of articulated human sdf. In *European Conference on Computer Vision*, 2022. 2, 3, 6
- [39] Chung-Yi Weng, Brian Curless, Pratul P. Srinivasan, Jonathan T. Barron, and Ira Kemelmacher-Shlizerman. HumanNeRF: Free-viewpoint rendering of moving people from monocular video. In *Proceedings of the IEEE/CVF Conference on Computer Vision and Pattern Recognition (CVPR)*, pages 16210–16220, 2022. 2
- [40] Guanjun Wu, Taoran Yi, Jiemin Fang, Lingxi Xie, Xiaopeng Zhang, Wei Wei, Wenyu Liu, Qi Tian, and Wang Xinggang. 4d gaussian splatting for real-time dynamic scene rendering. *arXiv preprint arXiv:2310.08528*, 2023. 2
- [41] Yiheng Xie, Towaki Takikawa, Shunsuke Saito, Or Litany, Shiqin Yan, Numair Khan, Federico Tombari, James Tompkin, Vincent Sitzmann, and Srinath Sridhar. Neural fields in visual computing and beyond. *Computer Graphics Forum*, 2022. 2
- [42] Qiangeng Xu, Zexiang Xu, Julien Philip, Sai Bi, Zhixin Shu, Kalyan Sunkavalli, and Ulrich Neumann. Point-nerf: Point-based neural radiance fields. In *Proceedings of the IEEE/CVF Conference on Computer Vision and Pattern Recognition*, pages 5438–5448, 2022. 2
- [43] Ziyi Yang, Xinyu Gao, Wen Zhou, Shaohui Jiao, Yuqing Zhang, and Xiaogang Jin. Deformable 3d gaussians for high-fidelity monocular dynamic scene reconstruction. *arXiv preprint arXiv:2309.13101*, 2023. 2, 7
- [44] Zeyu Yang, Hongye Yang, Zijie Pan, Xiatian Zhu, and Li Zhang. Real-time photorealistic dynamic scene representation and rendering with 4d gaussian splatting. *arXiv preprint arXiv 2310.10642*, 2023. 2
- [45] Zhengming Yu, Wei Cheng, xian Liu, Wayne Wu, and Kwan-Yee Lin. MonoHuman: Animatable human neural field from monocular video. In *CVPR*, 2023. 2
- [46] Zerong Zheng, Han Huang, Tao Yu, Hongwen Zhang, Yandong Guo, and Yebin Liu. Structured local radiance fields for human avatar modeling. In *Proceedings of the IEEE/CVF Conference on Computer Vision and Pattern Recognition (CVPR)*, 2022. 3, 5, 6, 1
- [47] Zerong Zheng, Xiaochen Zhao, Hongwen Zhang, Boning Liu, and Yebin Liu. Avatarrex: Real-time expressive full-body avatars. *ACM Transactions on Graphics (TOG)*, 42(4), 2023. 3

# Human Gaussian Splatting: Real-time Rendering of Animatable Avatars

## Supplementary Material

We present further analysis of our method. We invite readers to watch the video that summarizes our contributions and demonstrates real-time rendering, whose details are given in section 7. We further present extensive implementation details and hyperparameters setting in section 8, in order to facilitate the reproducibility of our experiments. Finally, we provide more qualitative results of our method on the THuman4 dataset in section 9.

### 7. Real-time video rendering

**Real-time rendering in the supplementary video** The attached video showcases real-time novel pose synthesis on the THuman4 dataset [46] at 60fps. This is done by extending the viewer from 3D-GS to dynamic scenarios in order to render videos. This frame rate is achieved by pre-computing the Gaussians in the observation space for each timestamp and caching it in the CPU memory. Then, real-time novel views can be rendered on any novel pose by loading the corresponding Gaussians in the GPU.

### 8. Reproducibility details

We have described our main implementation details in the main manuscript. In this section, we further report the hyperparameter values of our pipeline in Table 5. After that, we provide the additional implementation details of our approach, as described as below.

**Linear blend skinning** Our implementation for linear blend skinning (LBS) follows SMPL-X [26]. Notably, we do not use pose blend shapes before applying deformations on human joints, because the shape estimation and blend shapes obtained upon that may be inaccurate, thus we design MLP to handle pose-dependent deformations. We also remind that in our case, LBS is applied on canonical gaussians only and thus deforming template vertices is not necessary. The learnable per-gaussian skinning weights vector  $\mathbf{w}$  is a parameter optimized through gradient descent which can leads to negative values. We apply a ReLU activation on each  $w_j$  and then normalize the vector such that its components sum to 1 to obtain a well defined skinning weights vector. Finally, the transformations matrices  $\mathbf{M}_{j,t}$  that encode the rigid deformation of each body joint  $j$  for each training timestep  $t$  are precomputed before training to improve efficiency.

**Learning rates** Similar to 3D-GS [7], we use different learning rates for each set of learnable parameters. We leave

the learning rates of the original parameters (position, orientation, scaling, colors and opacity) unchanged. Our MLP and the skinning weights vectors  $\mathbf{w}$  are optimized with a constant learning rate that is set to  $1e^{-4}$ . For latent codes  $\mathbf{l}$ , we use a learning rate of  $2.5e^{-3}$ .

Table 5. Hyperparameters values.

Parameter name	Value
$\lambda_{L_1}$ (in Eqn. 8)	0.8
$\lambda_{\text{ssim}}$ (in Eqn. 8)	0.2
$\lambda_{\text{lpips}}$ (in Eqn. 8)	0.05
$\lambda_{\text{trans}}$ (in Eqn. 8)	0.01
$\lambda_{\text{rot}}$ (in Eqn. 8)	0.001
$\lambda_s$ (in Eqn. 8)	0.001
$\lambda_{\text{mesh}}$ (in Eqn. 8)	0.1
$\lambda_{\text{skn}}$ (in Eqn. 8)	0.001
Dimension of latent code $\mathbf{l}$	16

### 9. Qualitative analysis

We display in Figure 7 qualitative results of the HuGS method for subject01 and subject02 sequences from the THuman4 dataset [46] for novel pose synthesis. Note that no quantitative comparison is done on these subjects because the evaluation setup has not been released by the dataset authors. We observe that our method is able to fit the subjects with precise details, such as the black hood button (left picture) or the shoes (middle), and render the target body pose with high fidelity. However, we also showcase inaccuracies in the dataset caused by segmentation masks and motion blur that are observed regularly on training images and thus create artifacts in the learned model and degrade the overall rendering quality on these subjects.

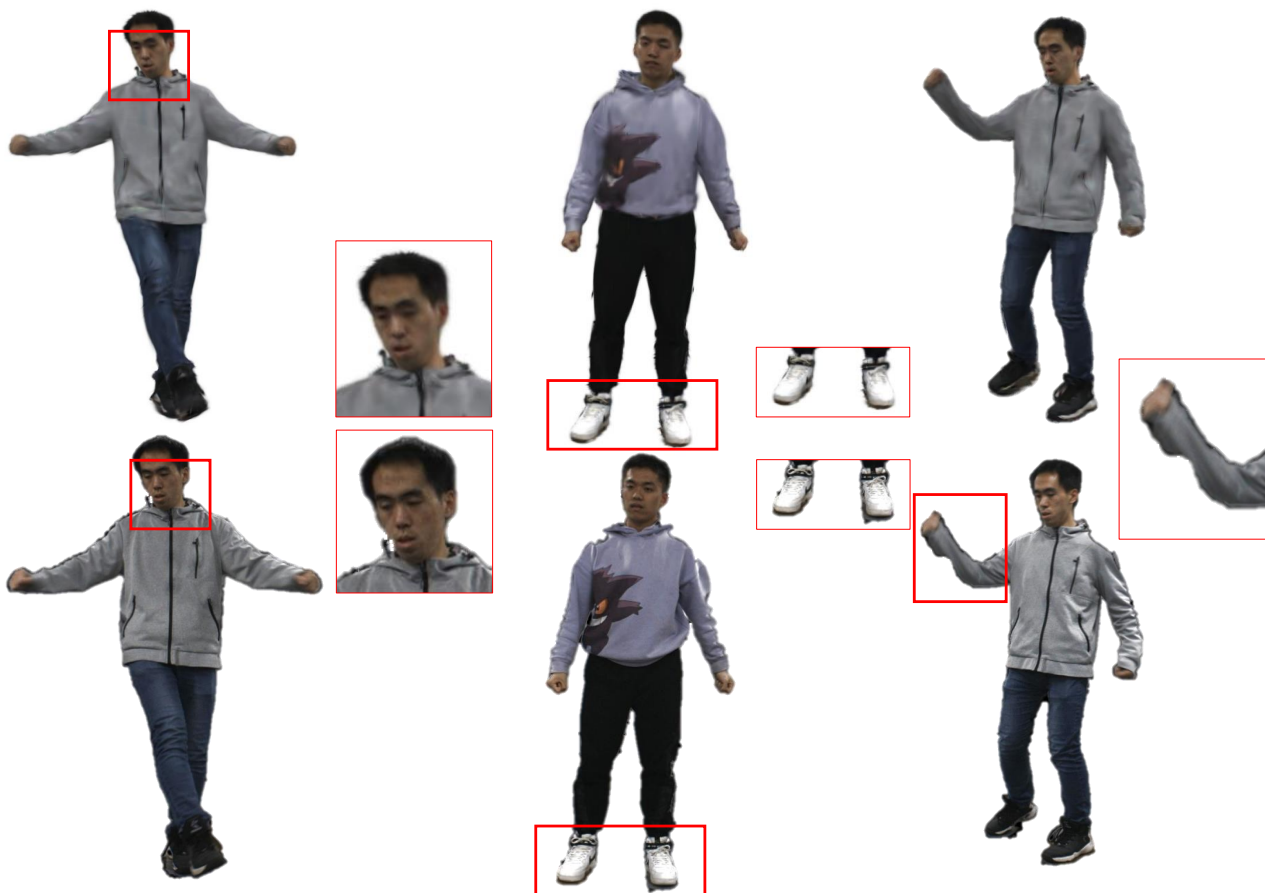


Figure 7. Qualitative visualization of HuGS novel pose synthesis on THuman4 dataset.